scientific reports

Check for updates

OPEN

Aggregation pathway complexity in a simple perylene diimide

Hyung Jun Kim[1,3,4], Changhwan Lee[2,5], P. James Schuck[2] & Laura J. Kaufman[1]✉

This study characterizes the influence of self-assembly conditions on the aggregation pathway and resulting photophysical properties of one-dimensional aggregates of the simple imide-substituted perylene diimide, *N*, *N*′-didodecyl-3,4,9,10-perylenedicarboximide (ddPDI). We show that ddPDI, which has symmetric alkyl chains at the imide positions, assembles into fibers with distinct morphology, emission spectra, and temperature-dependent behavior as a function of preparation conditions. In all conditions explored, aggregates are one-dimensional; however, assembly conditions can bias formation to either J-like or H-like aggregates. Specifically, a solvent phase interfacial (SPI) method yields two types of aggregates with distinct morphology and photophysical properties while a surface and solvent vapor assisted method (SSVA) generates more uniform aggregates with H-dominant behavior. A combined SPI and SSVA approach facilitates the simultaneous generation and in situ characterization of distinct ddPDI assemblies, some of which assemble via seeded growth. Microscopic and spectroscopic imaging unveil the heterogeneity among ddPDI aggregates, each with unique photophysical properties including H-dominant aggregates with a very high degree of molecular alignment and uniformity in intermolecular organization. Overall, this study highlights the pathway complexity in self-assembly of even the simplest PDI molecules, paving the way for utilization of simple PDI aggregates in applications that demand diverse photophysical behavior.

Perylene diimides (PDIs) are a versatile class of organic compounds with unique optical, electronic, and structural properties that make them promising materials for various optoelectronic applications, including solar cells and light emitting diodes[1–5]. As polycyclic aromatic molecules, they exhibit high thermal and chemical stability alongside strong absorption, near unity quantum yield, and high photostability, making them an excellent choice as single molecule emitters[6]. As molecules with polycyclic aromatic cores, self-assembly into one-dimensional structures via pi-pi stacking occurs readily. One-dimensional nanostructures, including nanowires, nanoribbons, and nanorods, are desirable for devices due to their small size, high surface area, and large aspect ratio that can induce directional behavior such as exciton diffusion, wave guiding, and charge transport[7–10]. Assemblies of PDIs have been used in diverse applications including biomolecule detection[11,12], pH change detection in cellular organelles[13], and energy conversion[14]. Given the PDI molecular core structure, pi-pi stacking dominates in simple PDIs, leading to one-dimensional aggregates dominated by H-aggregate character, showing a blue shift in absorption, weak emission, and high exciton diffusion efficiency[15,16].

To elicit particular photophysical behaviors in one-dimensional PDI aggregates, molecular complexity is often pursued, with substitutions (including asymmetric substitutions) at the bay and ortho positions alongside substitutions at the highly accessible imide positions[17,18]. Installing substituents at these positions can introduce additional competitive and/or cooperative non-covalent interactions alongside the dominant pi-pi stacking, producing aggregates with a diversity of photophysical properties, including those consistent with J-aggregation, such as strong emission and high charge mobility[15,16,19–21].

Here, we show that such diversity of photophysical behavior is available not only through molecular design but also through tuning assembly conditions. In particular, we demonstrate that several types of one-dimensional aggregates can be prepared from a simple imide-substituted PDI molecule. Typically, aggregates of PDIs are prepared through solution-based assembly, in which monomers dispersed in a good solvent are rapidly introduced to poor solvent, inducing aggregation[7]. In this approach, the concentration of the PDI, the solvents used, and their relative proportions can be altered, which can lead to differences in aggregation kinetics, molecular packing, and final aggregate morphology and photophysics[22–25]. Despite allowing for some tuning of aggregate assembly, such solution based aggregation induction is relatively poorly controlled, often leading to heterogeneity in aggregate properties and limited reproducibility between experiments. More controlled,

[1]Department of Chemistry, Columbia University, New York, NY 10027, USA. [2]Department of Mechanical Engineering, Columbia University, New York, NY 10027, USA. [3]Present address: Department of Chemistry, Massachusetts Institute of Technology (MIT), Cambridge, MA 02139, USA. [4]Broad Institute of MIT and Harvard, Cambridge, MA 02139, USA. [5]Department of Materials Science and Engineering, Korea Advanced Institute of Science and Technology (KAIST), 34141 Daejeon, Republic of Korea. ✉email: kaufman@chem.columbia.edu

bottom-up approaches have also been demonstrated for the preparation of 1D nanofibers on substrates, with final aggregate structures and properties dependent on factors including molecular structure, solvent, substrate properties, and post-assembly treatment[7]. Here, we demonstrate that a bottom-up approach via controlled solvent vapor delivery to surface adsorbed monomers leads to highly organized, homogeneous assemblies of *N*, *N*'-didodecyl-3,4,9,10-perylenedicarboximide (ddPDI) while also facilitating in situ characterization of the self-assembly. We also show that this approach can be used to direct aggregate growth from pre-prepared seeds. Such seeded assembly can provide access to a variety of structures not accessible using other approaches, as has been shown in other types of molecules and with differing approaches to preparing seeds[26–34]. In particular, we show that controlled delivery of chloroform to monomeric ddPDI and/or small oligomeric ddPDI seeds can be used to produce 3 types of one-dimensional assemblies, two of which are dominated by H-like character and one of which is dominated by J-like character, behavior not previously demonstrated with simple imide-substituted PDIs.

Experimental details

Materials

N, *N*'-didodecyl-3,4,9,10-perylenedicarboximide (ddPDI) (Fig. 1a) was synthesized following the procedure reported in the literature[35]. The starting materials and all solvents were obtained from Sigma-Aldrich and Thermo Fisher Scientific and used without further purification.

Aggregate preparation

Solvent phase interfacial (SPI) (self-)assembly is described in detail elsewhere[7]. Briefly, concentrated PDI solutions were prepared in chloroform at high (1 mM) or low (100 μM) concentration. A small volume of PDI solution was injected into a large volume of methanol in a vial resulting in methanol-chloroform mixtures with a liquid volume ratio of 90:10%. This resulted in a 10-fold dilution of the initial PDI solution. Aggregates became visible to the naked eye via turbidity in the solution within several minutes. Over several days, precipitate

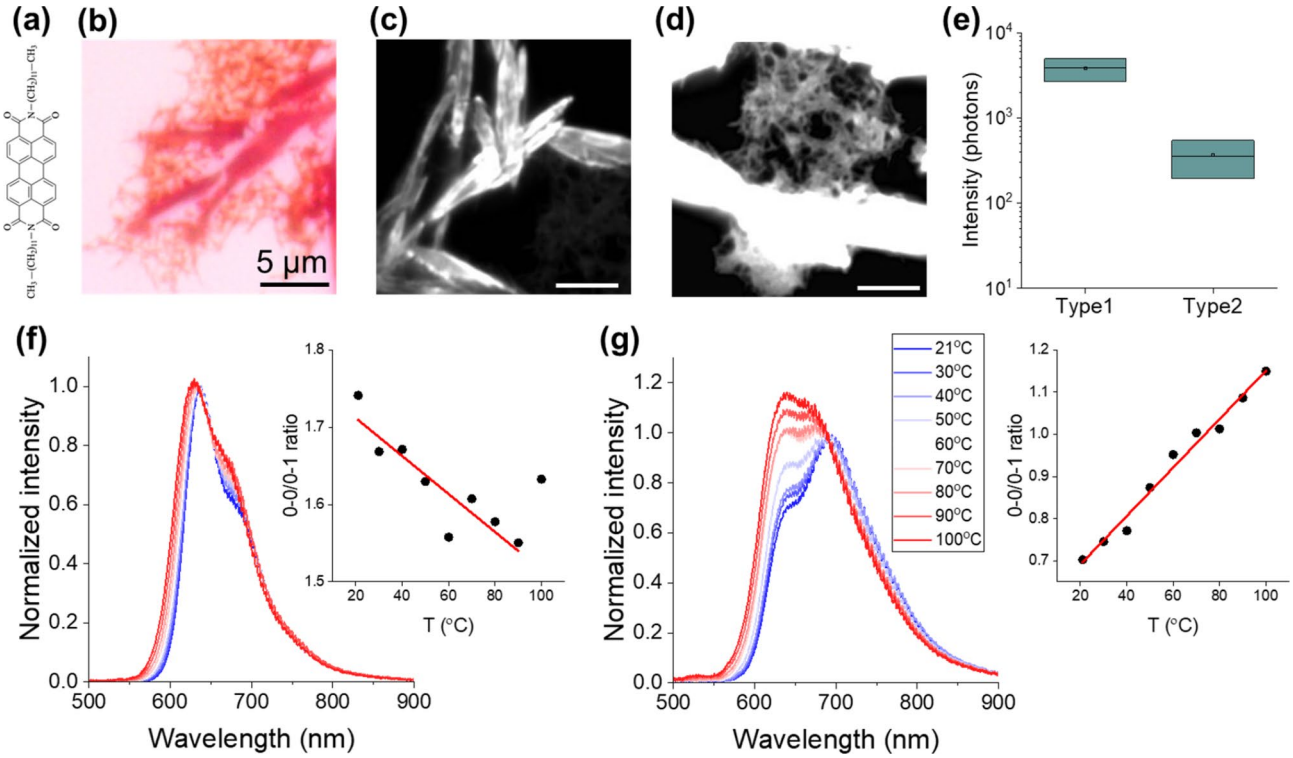

Fig. 1. (**a**) Molecular structure of *N*, *N*'-didodecyl-3,4,9,10-perylenedicarboximide (ddPDI). (**b**–**d**) ddPDI aggregates prepared via solvent phase interfacial self-assembly in a mixture of chloroform and methanol and spin-cast onto a glass coverslip. Scale bar is 5 μm in each image. (**b**) Bright-field image reveals two types of aggregates, one of which is thick and invariably straight (type 1) and one of which is thin and displays curvature (type 2). (**c**,**d**) Fluorescence images of (**c**) type 1 and (**d**) type 1 and 2 ddPDI aggregates. In (**d**), the intensity range displayed is set to show emission from type 2 aggregates, leading to saturation in emission from type 1 aggregates. (**e**) Intensity per pixel averaged over 50 frames of diffraction limited spots on different aggregates for type 1 and type 2 aggregates. Box plots show median (line), mean (symbol) and ± 1 standard deviation. (**f**,**g**) Temperature dependent-fluorescence spectra of (**f**) type 1 and (**g**) type 2 ddPDI aggregates. Spectra are normalized to the dominant vibronic peak position at room temperature (the 0–0 peak in type 1 and the 0–1 peak in type 2 aggregates). Insets in (**f**) and (**g**) show the 0–0/0–1 peak height ratio as a function of temperature with best fit line to the data. Legend in (**g**) also applies to (**f**).

settled to the bottom of the vials. A schematic depiction of the process is shown in Fig. S1a. For microscopic characterization of such aggregates, the aggregates were drop-cast onto a glass substrate and subjected to spinning at 1500 rpm for several seconds to remove residual solvent.

The self-assembly approach we term surface and solvent vapor assisted (self-)assembly (SSVA) is shown schematically in Fig. S1b. Here, 10 μM PDI in chloroform solution was spin-coat three times, utilizing one drop for each coating, onto a glass coverslip at 1500 rpm. The substrates were then exposed to nitrogen gas flow for approximately 60 min to remove residual solvent. Next, chloroform solvent vapor was directed to the sample and the surface was exposed to this vapor for 20 min with 150–250 sccm flow rate. The solvent-exposed sample was then again exposed to nitrogen gas flow for 60 min to arrest the process and remove any residual solvent. This experimental setup, described in detail in Ref.[36], allows in situ monitoring of the self-assembly process.

In the seeded growth assembly process, the two processes described above were combined. First, the chloroform-based PDI solution was injected into methanol as described in the high concentration SPI approach. Within one minute, in the early stages of the self-assembly process, this solution was spin-cast onto a glass coverslip three times. The small aggregates presumed to be present were intended to serve as seeds for aggregate growth. Following deposition of the putative seeds, 10 μM PDI stock solution was spin-coat onto the glass coverslip containing the seed aggregates two times, intended to provide a pool of monomers as in the SSVA process. The resulting sample contained both seed aggregates and individual PDI molecules dispersed on the glass surface (*vide infra*). The same procedure described in the SSVA approach - in which nitrogen, chloroform, and nitrogen were delivered to the sample in series - was then carried out.

All samples were prepared at room temperature (≈21 °C) and all experiments were performed at room temperature unless otherwise specified.

Ensemble absorption and fluorescence measurements

Ensemble absorption and emission spectra in solution were obtained on a UV-vis spectrophotometer (Agilent 8453) and fluorometer (Horiba QM-800) at room temperature. For absorption, the excitation source was a tungsten lamp, which covers the range of 370–1100 nm. For fluorescence measurements, 488 nm excitation was used. In both absorption and fluorescence, spectral resolution is below 4 nm.

Microscopic analysis

Imaging was performed using a home-built microscope with a 488 nm continuous-wave diode laser (Thorlabs, L488P60) as the excitation source. To ensure uniform illumination of the field of view, the laser beam was coupled into a multimode fiber and mechanically shaken. Circularly polarized light was generated with a combination of a half-wave plate and a quarter-wave plate, and then directed onto the back-focal plane of an oil immersion objective (Olympus, UAPON100XOTIRF, NA = 1.49) to achieve wide-field illumination. The fluorescence emitted was collected by the same objective filtered using a 496 nm long pass filter (Semrock, BrightLine Fluorescence Edge 496/LP FF01-496/LP-25) and detected using an EMCCD camera (Andor, iXon Ultra 888 DU-888U3-CS0-#BV). All movies were captured as 16-bit images over 401 × 401 pixels, corresponding to a 36.5 × 36.5 μm field of view.

For comparison of fluorescence intensity across samples, series of 50-frame movies were recorded with an exposure time of 100 ms per frame. Excitation intensity was set to ≈30 mW/cm^2 at the sample and the same EM gain was used for all samples. Intensity was converted from counts to photons using Solis software (Andor version 4.29). All frames in each movie were then averaged to generate fluorescence images, and intensity distributions were obtained. Briefly, representative areas of 7 × 7 pixels on PDI aggregates were selected and intensity was determined by averaging the 5 pixels with maximum intensity from each selected area. For the intensity measurements associated with polarization modulation measurements, 10 frame movies with an exposure time of 200 ms per frame and higher EM gain were used.

To measure polarization modulation, which reports on alignment of transition dipoles in a system, a rotating linear polarizer was added to the excitation beam path, and fluorescence intensity measurements were taken as a function of polarization angle. The polarizer was rotated at a rate of 10°/s. The illumination intensity was ≈100 mW/cm^2, with excitation intensity variation of ± 5% as a function of polarization angle due to imperfect optical alignment. The polarization modulation was expressed as $I(\phi) = I_0[1 + M\cos[2(\phi - \phi_0)]]$, where $I(\phi)$ is the fluorescence intensity as a function of ϕ, the polarization angle of the excitation light. I_0 is the average fluorescence intensity, and ϕ_0 is a reference polarization angle corresponding to the maximum intensity. M values, which may vary from 0 to 1, were extracted by fitting the angle-dependent intensity with data analysis performed as described in Reference 37.

Photoluminescence spectral measurements were performed as described in detail previously[38]. Briefly, these measurements were performed using an inverted confocal microscope: the excitation source was a 488 nm fs-pulsed laser with a line filter and waveplates to create circularly polarized light. The excitation light was directed into an oil immersion objective (Olympus, UAPON100XOTIRF, NA = 1.49) and focused onto the sample, which was on a three-dimensional nano-scanning piezo stage. Emitted signal was collected through the same objective, filtered by long pass filters (Thorlabs, FELH0500 and Semrock, BrightLine Fluorescence Edge 496/LP FF01-496/LP-25), and directed towards a spectrometer equipped with an EM-CCD. The temperature of the glass substrates was controlled using a micro heating system (Interherence GmbH, VAHEAT standard range version)[39]. Temperature calibration was performed according to the manufacturer's directions for each substrate used, and the PL measurements were conducted at constant temperatures between 21 and 100 °C. For measurements taken above room temperature, to mitigate thermal effects, an air objective lens (Nikon, MUT10101, 100X, NA = 0.95) was used instead of an oil immersion objective.

Brightfield imaging was conducted on the confocal microscope also used for PL spectral measurements. The excitation was achieved with a while light LED (Thorlabs, MNWHL4) and the reflected photons were filtered by

long pass filters (Thorlabs, FELH0500 and Semrock, BrightLine Fluorescence Edge 496/LP FF01-496/LP-25) and detected on a CMOS camera (AmScope, MU503).

Results

Aggregates prepared via solvent phase interfacial self-assembly

Samples prepared via SPI typically revealed two types of aggregates with distinct morphology (Fig. 1b), an observation that suggested even this simple ddPDI molecule may show multiple aggregation pathways. While both types of aggregates are one-dimensional structures with large aspect ratio, one type (referred to as type 1) is thick and rigid, being invariably straight, while the other type (referred to as type 2) appears thinner and more flexible, given curvature that is apparent over several microns. These aggregates also exhibit significant difference in photophysical behaviors, particularly in fluorescence intensity. Average brightness per pixel of these two types of aggregates differ by nearly a factor of 10, with type 1 aggregates much brighter than type 2 (Fig. 1d,e). The difference in emission intensity per pixel between the two types of aggregates may suggest more quenching and H-aggregate character in type 2 aggregates relative to type 1 aggregates.

Absorption and emission spectra reinforce this suggestion. The spectra of ddPDI molecules dispersed in solution (Fig. S2a) show symmetric absorption and emission typical of the core of the PDI molecule, with dominant absorption at ≈525 nm and emission at ≈535 nm, as expected given that alkyl substitutions at the imide position have negligible effect on electronic properties of PDI molecules[33]. PDI assemblies, in contrast, show more complex spectra. While scattering in the solution and sedimentation of the aggregates make it challenging to collect ensemble absorption and fluorescence spectra during the entirety of the aggregation process, absorption and fluorescence spectra collected early in the assembly process show interesting features (Fig. S2b). In particular, the absorption spectrum shows split asymmetric bands, consistent with PDI systems with hybrid H- and J-like contributions[16], while the fluorescence spectrum shows emergence of a broad red-shifted peak. Further insight emerges from fluorescence measurements collected locally from the different types of aggregates (Figs. 1f,g; S2c). Here, at room temperature, type 1 aggregates display a dominant 0–0 peak at ≈635 nm while type 2 aggregates display an enhanced 0–1 vibronic peak at ≈690 nm. This is consistent with more J-like character (associated with short-range coupling) in the type 1 aggregates and more H-like character (associated with longer range coupling) in the type 2 aggregates[40,41].

Temperature dependent measurements of emission spectra, conducted over a previously unexplored range of 20–100 °C, provide additional insights into the photophysical behavior of PDI aggregates. To the best of our knowledge, this is the first such measurement on aggregates in this temperature range, bridging the gap between studies conducted at cryogenic temperatures and room temperature. These measurements reveal behavior consistent with that described for H- and J-dominant aggregate behavior in other PDI systems at lower temperatures[16]. Specifically, spectra from type 1 aggregates consistently display a dominant 0–0 vibronic peak and show little variation with temperature (Fig. 1f), a characteristic pointed out previously in aggregates that have characteristics of both H- and J-behavior but are dominated by J-character, thus termed hJ aggregates. In contrast, the 0–0/0–1 ratio in type 2 aggregates shows notable increase as temperature increases (Fig. 1g), behavior previously shown for Hj aggregates (aggregates with H and J character showing dominant H-like behavior). Notably, neither type of aggregate shows signs of disassembly (via increase in fluorescence signatures associated with monomers) in these experiments. The spectral trend differences as a function of temperature were previously attributed to differences in slip stacking arrangement in aggregates composed of different PDIs[16]. Specifically, increased 0–0/0–1 ratio with increasing temperature was attributed to positive Coulomb coupling in H-dominant aggregates while the persistence of a dominant 0–0 peak was ascribed to enhanced counteracting charge transfer-mediated coupling as occurs in J-dominant aggregates, with the details of Coulomb coupling and charge transfer-mediated coupling determined by the pi-stacking orientation and the distance between PDI backbones.

Performing the same SPI self-assembly at an initial PDI concentration one tenth of that used in the experiments described above resulted in a single type of aggregate. Figure S3 shows a representative fluorescence image and emission spectra of these aggregates as a function of temperature. Morphologically, the aggregates resemble type 2 aggregates shown in Fig. 1, as they display uniform width and show curvature, though they are longer than those seen in the higher concentration preparation. Their emission spectra at room temperature show relatively strong 0–0 and 0–1 peaks, and there is a positive linear correlation between temperature and 0–0/0–1 peak ratio, similar to that seen in the H-dominant type 2 aggregates as shown in Fig. 1g. At this lower concentration, PDI assembly occurs more slowly and this may allow sufficient time for the formation of parallel aligned molecular organization of the long alkyl substituents that may otherwise create steric hindrance that inhibits organization into a more thermodynamically favorable structure in which the pi-pi interaction of PDI cores is maximized[25].

Aggregates prepared via surface and solvent vapor assisted assembly

Spin-cast ddPDI monomers on a glass substrate were exposed to solvent vapor flow to facilitate self-assembly as described in Experimental Details and shown schematically in Fig. S1b. We hypothesize the delivery of chloroform conveys mobility to the monomers, rapidly depleting free monomer from the surface causing spontaneous phase separation into solute-rich microdroplets (Fig. S4). While chloroform is generally considered a good solvent for PDIs, some aggregation is known to occur in chloroform for PDIs with linear alkyl chains at the imide positions[42], and the high concentration of ddPDI in the microdroplets may facilitate assembly.

Fluorescence images and spectra of the resulting aggregates are shown in Fig. 2. As in aggregates prepared via SPI, aggregates prepared via SSVA display anisotropic one-dimensional structure. These aggregates show limited curvature and appear quite homogeneous in width, length, and brightness relative to aggregates prepared via SPI. Aggregates prepared via SSVA exhibit similar vibronic bands to the 0–0 and 0–1 transitions of SPI-prepared

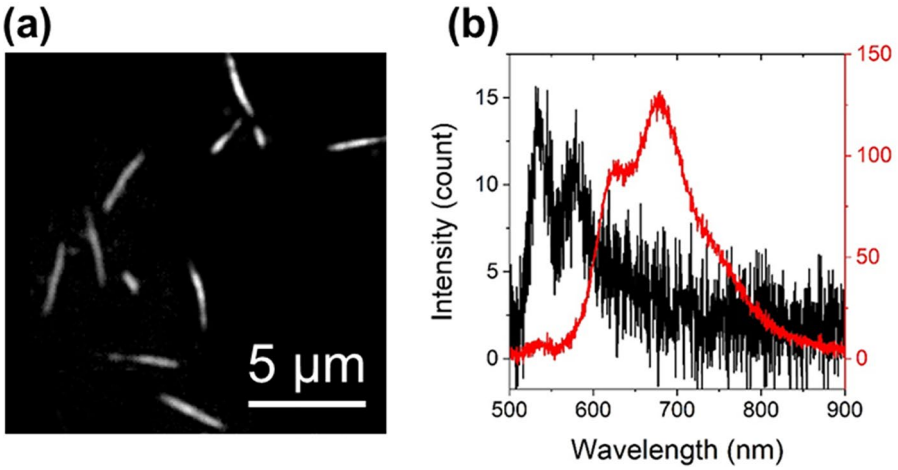

Fig. 2. ddPDI aggregates prepared via SSVA. (**a**) Fluorescence image of aggregates and (**b**) fluorescence spectra of aggregates (red) as well as an area of the coverslip with no obvious aggregates (black).

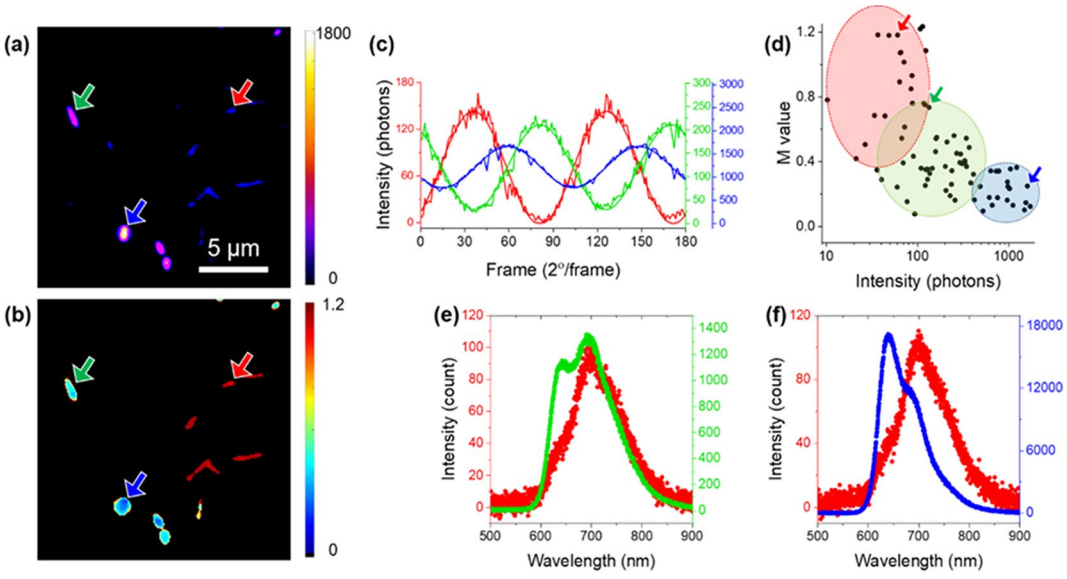

Fig. 3. Characterization of ddPDI aggregates prepared via combined SPI and SSVA. (**a**) Fluorescence intensity heatmap image and (**b**) modulation depth (M) heatmap image of ddPDI aggregates. (**c**) Representative intensity modulation traces with fits of ddPDI aggregates for putative H-dominant aggregates originating from SSVA alone (red), H-dominant aggregates originating from seeded growth (green), and J-dominant aggregates originating from seeded growth (blue). (**d**) M values vs. fluorescence intensities for each assessed aggregate. Ellipses are drawn by eye and suggest 3 groupings distinguished by final intensity as well as M value, with colors corresponding to those in (**c**). Arrows correspond to the aggregates identified with arrows of the same color in (**a**) and (**b**). (**e**,**f**) Representative emission spectra of H-dominant aggregates originating from the SSVA process (red), H-dominant aggregates originating from seeded growth (green), and J-dominant aggregates originating from seeded growth (blue). Each pair presented in (**e**) and (**f**) were collected in the same field of view.

aggregates. The SSVA aggregates exhibit a relatively enhanced 0–1 peak at room temperature, and their spectral shape closely resembles that of SPI aggregates generated under lower concentration conditions, consistent with H-dominant aggregate photophysics. Emission spectra collected from regions without aggregates reveal low intensity emission consistent with that of monomers (Figs. 3b, S5). This suggests the SSVA aggregates are formed through the assembly of such single molecules, rather than small aggregates that may be present in the stock solution or after spin-casting the stock solution.

Aggregates prepared via seeded growth

To potentially generate and characterize multiple types of ddPDI assemblies simultaneously as well as to explore the outcome of seeded growth, we combined the SPI and SSVA approaches. In essence, we arrested solvent phase interfacial (SPI) aggregation at an early time point and deposited aggregates present at that time to serve as potential seeds for monomeric ddPDI that was deposited on the substrate via the SSVA procedure, with solvent vapor delivered as described in Experimental Methods. In situ optical imaging during the aggregate growth process was performed. In particular, we assessed aggregate size at multiple time points in videos recorded over 20 min during solvent vapor delivery to characterize aggregate growth in length over time. While some aggregates grew from initially apparent bright features, presumed to be small seed aggregates from the SPI assembly, some grew from areas that initially appeared dark, i.e. presumably from monomers that did not emit sufficiently strongly to be obvious at the same settings used to image the seeds. We categorized aggregates into two groups, seeded growth and SSVA-only (monomer initiated) growth, based on the brightness of each feature in the initial 10 frames of the movie. The mean growth rate in length of SSVA-only aggregates was greater than that of seeded aggregates (Fig. S6). This may occur because the seeded aggregates are wider and require more monomers to be added in cross-section to gain length.

Following assembly, microscopic and spectroscopic imaging were employed to characterize the ddPDI aggregates that result from the combined preparation approach. Differences between the two types of aggregates (seeded growth vs. monomer-initiated growth) in shape and intensity are observed, suggesting different degrees of quenching in each type of aggregate[43,44]. To assess possible origins of these differences, we performed polarization modulation measurements under the rotation of linear polarization excitation, as such measurements report the alignment of transition dipoles in the probed region[37]. We assessed the correlation between fluorescence intensity and polarization modulation depth (M) for ddPDI aggregates, and representative results are shown in Fig. 3a–c. M values may vary between 0 and 1, where a value close to 1 indicates highly aligned and unidirectional arrangement of transition dipoles in the interrogated region while a value close to 0 suggests a random transition dipole arrangement in the interrogated region of the aggregate. Figure 3a,b reveal that the aggregates with high intensity tend to have low M values and vice versa. Moreover, aggregates with high M values tend to be of uniform size and (low) intensity. Based on the robust correlation between intensity and modulation depth observed and previous findings in this study, we categorize the assembled aggregates into three groups: two groups originating from seeds prepared in the solvent phase interfacial (SPI) process and one from the surface and solvent vapor assisted (SSVA) process alone. Aggregates exhibiting the highest fluorescence intensity displayed a dominant 0–0 peak and the lowest M values, consistent with J-dominant aggregates that are expected to have increased distance between and/or relatively poor organization among the ddPDI molecules. Conversely, aggregates with relatively lower intensity showed an enhanced 0–1 peak, suggesting H-dominant properties. We note that both H and J-aggregates result from seeded growth, suggesting that both types of aggregates seen in high concentration SPI approaches (Fig. 1) can result from seeds assembled in early stages of the self-assembly process. Interrogating aggregate assembly directly in SPI is not possible given the bulk, uncontrolled approach; however, here capturing seeds from the early self-assembly process allows direct interrogation of the growth and photophysical properties of such aggregates during their assembly.

In sum, with the combined SPI/SSVA approach, three types of aggregates are produced, two of which show primarily H-dominant characteristics and one showing J-dominant character. Within the category of H-dominant aggregates, those that result solely from the bottom-up growth process initiated from a single molecule through solvent vapor delivery exhibit uniform morphology and exceptionally high M values along with an enhanced 0–1 vibronic peak. These characteristics indicate a high degree of alignment of the transition dipoles and molecular organization.

Discussion

In this study, we explored and directed the self-assembly of ddPDI molecules into one-dimensional structures with distinct morphology and photophysical characteristics, as summarized in Fig. 4. At high concentrations, solvent phase interfacial assembly resulted in two types of aggregates, one with J-dominant and one with H-dominant behavior, with notable differences in morphology, brightness, and spectral characteristics. These differences in behavior are consistent with variations in slip stacking arrangements within the aggregates, and to the best of our knowledge this is the first demonstration of J-dominant one-dimensional PDI-based aggregates prepared from simple linear hydrocarbon imide-substituted PDIs. We hypothesize that under these conditions, in which self-assembly occurs rapidly, the ddPDI molecules sometimes assemble into well-organized thermodynamically stable structures but also can form kinetically controlled structures with poorer stacking and J-dominant photophysical behavior. In contrast, SPI conducted at a lower concentration resulted solely in aggregates displaying a set of characteristics consistent with H-dominant aggregates, including a positive correlation between the 0–0/0–1 peak ratio and temperature. Under such lower concentration conditions, self-assembly is slowed and the molecules apparently form parallel-aligned structure with the linear alkyl chain substituents providing minimal steric hindrance and potentially facilitating cooperative interchain interactions beyond the pi-pi stacking between PDI core backbones[25,45].

Surface-assisted solvent vapor annealing of ddPDI molecules on a glass substrate generated aggregates with similar spectral characteristics, and similar H-dominant behavior, to those produced by SPI under lower concentration conditions. A combined approach, in which SPI seed aggregates are deposited and SSVA is then applied, allowed preparation and characterization of all three types of assemblies observed in isolated approaches simultaneously. Microscopic and spectroscopic imaging of ddPDI aggregates prepared with this combined approach revealed heterogeneity in terms of fluorescence intensity and modulation depth (M) distribution, which reports on molecular alignment. Both aggregates grown solely via SSVA and aggregates resulting from seeded growth were present in this mixture. From seeded growth, some aggregates showed J-dominant behavior,

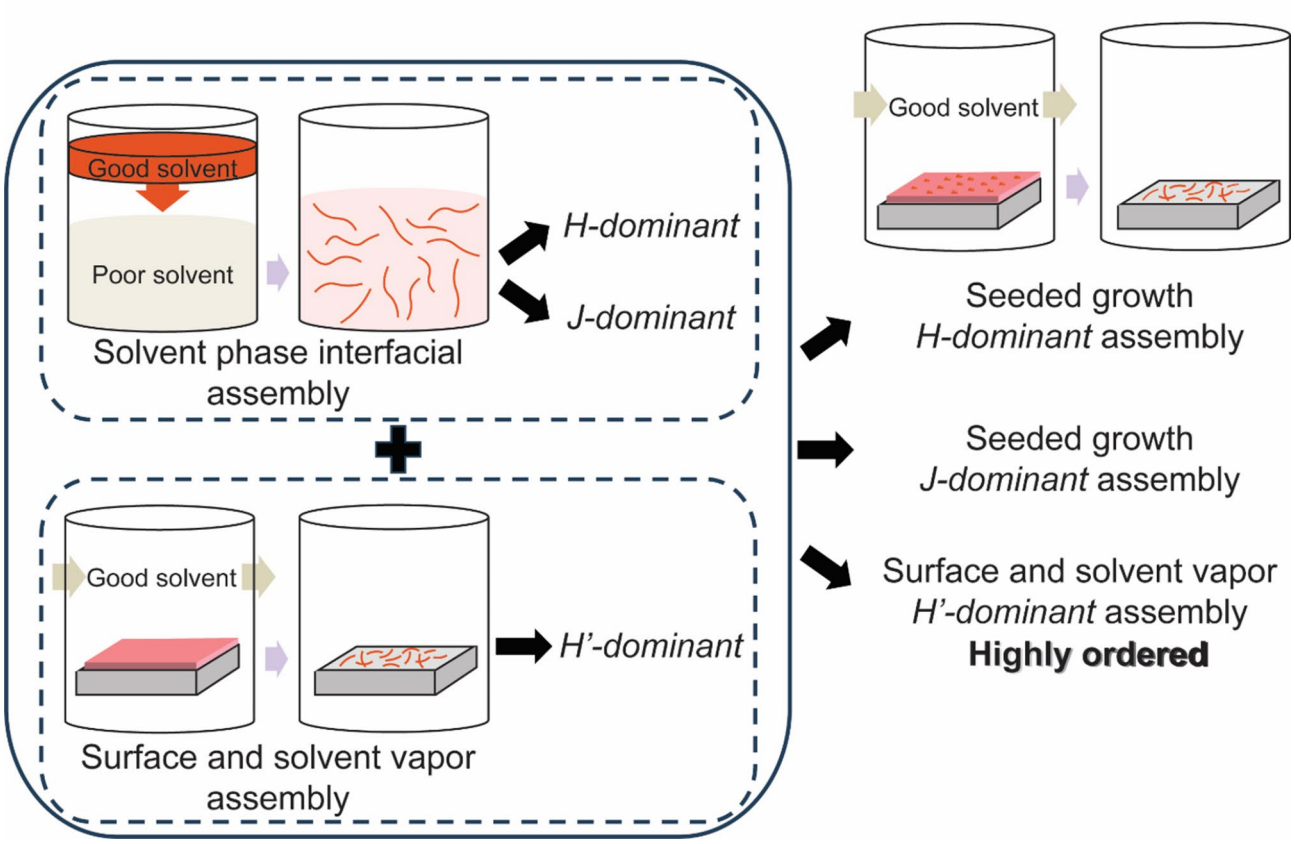

Fig. 4. Aggregation pathways of ddPDI. Solvent phase interfacial (SPI) assembly yields two types of aggregates with distinct morphology and photophysical properties while a surface and solvent vapor assisted method (SSVA) generates uniform aggregates with H-dominant behavior. A combined SPI and SSVA approach facilitates the simultaneous generation and in situ characterization of three distinct types of assemblies.

with high fluorescence intensity and a dominant 0–0 peak as well as low *M* values indicating limited molecular alignment, while others show lower intensity, an enhanced 0–1 peak, and higher *M* values. Notably, H-dominant aggregates resulting from the bottom-up growth process from SSVA without evidence of seeded growth exhibited exceptional alignment, suggesting uniformity in intermolecular arrangement.

Conclusion

In summary, this study provides insight into the diverse pathways and factors that influence the formation of assemblies of even the simplest PDI molecules, demonstrating methods with which to direct their morphological and photophysical characteristics as well as showing that both J- and H-dominant aggregates can be prepared from a simple symmetric imide-substituted PDI molecule.

Data availability

The data supporting the findings of this study are available within the paper and its Supplementary Information files. Raw data is available from the corresponding author upon reasonable request.

Received: 26 September 2024; Accepted: 16 December 2024
Published online: 30 December 2024

References

1. Huang, C., Barlow, S. & Marder, S. R. Perylene-3,4,9,10-tetracarboxylic acid diimides: synthesis, physical properties, and use in organic electronics. *J. Org. Chem.* **76**, 2386–2407 (2011).
2. Lin, Y. Z. et al. A star-shaped perylene diimide electron acceptor for high-performance organic solar cells. *Adv. Mater.* **26**, 5137–5142 (2014).
3. Wu, N. et al. Persistent photoconductivity in perylene diimide nanofiber materials. *ACS Energy Lett.* **1**, 906–912 (2016).
4. Naqvi, S., Kumar, M. & Kumar, R. Facile synthesis and evaluation of electron transport and photophysical properties of photoluminescent PDI derivatives. *ACS Omega.* **4**, 19735–19745 (2019).
5. Masoomi-Godarzi, S. et al. Competitive triplet formation and recombination in crystalline films of perylenediimide derivatives: Implications for singlet fission. *J. Phys. Chem. C.* **124**, 11574–11585 (2020).
6. Wurthner, F. Perylene bisimide dyes as versatile building blocks for functional supramolecular architectures. *Chem. Commun.*, 1564–1579 (2004).

7. Chen, S., Slattum, P., Wang, C. Y. & Zang, L. Self-assembly of perylene imide molecules into 1d nanostructures: Methods, morphologies, and applications. *Chem. Rev.* **115**, 11967–11998 (2015).
8. Wu, S., Zhou, B. & Yan, D. Recent advances on molecular crystalline luminescent materials for optical waveguides. *Adv. Opt. Mater.* **9**, 2001768 (2021).
9. Kim, Y. J. et al. Hierarchical self-assembly of perylene diimide (PDI) crystals. *J. Phys. Chem. Lett.* **11**, 3934–3940 (2020).
10. Kumar, S. et al. Exciton annihilation in molecular aggregates suppressed through quantum interference. *Nat. Chem.* **15**, 1118–1126 (2023).
11. Roy, R., Sajeev, N. R., Sharma, V. & Koner, A. L. Aggregation induced emission switching based ultrasensitive ratiometric detection of biogenic diamines using a perylenediimide-based smart fluoroprobe. *ACS Appl. Mater. Inter.* **11**, 47207–47217 (2019).
12. Wu, J., Peng, M., Mu, M., Li, J. & Yin, M. Perylene diimide supramolecular aggregates: Constructions and sensing applications. *Supramolecular Mater.* **2**, 100031 (2023).
13. Keum, C., Hong, J. Y., Kim, D., Lee, S. Y. & Kim, H. Lysosome-instructed self-assembly of amino-acid-functionalized perylene diimide for multidrug-resistant cancer cells. *ACS Appl. Mater. Inter.* **13**, 14866–14874 (2021).
14. Peurifoy, S. R. et al. Three-dimensional graphene nanostructures. *J. Am. Chem. Soc.* **140**, 9341–9345 (2018).
15. Hestand, N. J. & Spano, F. C. Molecular aggregate photophysics beyond the kasha model: novel design principles for organic materials. *Acc. Chem. Res.* **50**, 341–350 (2017).
16. Oleson, A. et al. Perylene diimide-based Hj- and hJ-aggregates: The prospect of exciton band shape engineering in organic materials. *J. Phys. Chem. C.* **123**, 20567–20578 (2019).
17. Marin, F., Zappi, A., Melucci, D. & Maini, L. Self-organizing maps as a data-driven approach to elucidate the packing motifs of perylene diimide derivatives. *Molec Sys Des. Eng.* **8**, 500–515 (2023).
18. Würthner, F. et al. Perylene bisimide dye assemblies as archetype functional supramolecular materials. *Chem. Rev.* **116**, 962–1052 (2015).
19. Zhan, X. W. et al. Rylene and related diimides for organic electronics. *Adv. Mater.* **23**, 268–284 (2011).
20. Schaack, C., Evans, A. M., Ng, F., Steigerwald, M. L. & Nuckolls, C. High-performance organic electronic materials by contorting perylene diimides. *J. Am. Chem. Soc.* **144**, 42–51 (2022).
21. Fink, R. F. et al. Exciton trapping in pi-conjugated materials: a quantum-chemistry-based protocol applied to perylene bisimide dye aggregates. *J. Am. Chem. Soc.* **130**, 12858–12859 (2008).
22. El-Khouly, M. E., El-Refaey, A., Shaban, S. Y. & El-Kemary, M. Optical properties and structural morphology of one-dimensional perylenediimide derivatives. *J. Lumin.* **196**, 455–461 (2018).
23. Shahar, C. et al. Precrystalline Aggregates Enable Control over Organic Crystallization in Solution. *Angew Chem. Int. Ed.* **55**, 179–182 (2016).
24. Chen, Z. J. et al. Photoluminescence and conductivity of self-assembled pi-pi stacks of perylene bisimide dyes. *Chem. Eur. J.* **13**, 436–449 (2007).
25. Balakrishnan, K. et al. Effect of side-chain substituents on self-assembly of perylene diimide molecules: Morphology control. *J. Am. Chem. Soc.* **128**, 7390–7398 (2006).
26. Fukui, T. et al. Seeded self-assembly of charge-terminated poly(3-hexylthiophene) amphiphiles based on the energy landscape. *J. Am. Chem. Soc.* **142**, 15038–15048 (2020).
27. Liu, Y. et al. Emergent self-assembly pathways to multidimensional hierarchical assemblies using a hetero-seeding approach. *Chem. – Eur. J.* **25**, 13484–13490 (2019).
28. Liu, Y. et al. Two-dimensional seeded self-assembly of a complex hierarchical perylene-based heterostructure. *Angew Chem. Int. Ed.* **56**, 11380–11384 (2017).
29. MacFarlane, L. R., Li, X., Faul, C. F. J. & Manners, I. Efficient and controlled seeded growth of poly(3-hexylthiophene) block copolymer nanofibers through suppression of homogeneous nucleation. *Macromolecules* **54**, 11269–11280 (2021).
30. Ogi, S., Stepanenko, V., Sugiyasu, K., Takeuchi, M. & Würthner, F. Mechanism of self-assembly process and seeded supramolecular polymerization of perylene bisimide organogelator. *J. Am. Chem. Soc.* **137**, 3300–3307 (2015).
31. Wagner, W., Wehner, M., Stepanenko, V. & Würthner, F. Supramolecular block copolymers by seeded living polymerization of perylene bisimides. *J. Am. Chem. Soc.* **141**, 12044–12054 (2019).
32. Biran, I. et al. Organic crystal growth: hierarchical self-assembly involving nonclassical and classical steps. *Cryst. Growth. Des.* **22**, 6647–6655 (2022).
33. Wilson-Kovacs, R. S., Fang, X., Hagemann, M. J. L., Symons, H. E. & Faul, C. F. J. Design and control of perylene supramolecular polymers through imide substitutions. *Chem. Eur. J.* **28**, (2022).
34. Wehner, M. & Würthner, F. Supramolecular polymerization through kinetic pathway control and living chain growth. *Nat. Rev. Chem.* **4**, 38–53 (2020).
35. Demmig, S. & Langhals, H. Leichtlösliche, lichtechte Perylen-Fluoreszenzfarbstoffe. *Chem. Ber.* **121**, 225–230 (2006).
36. Yang, J., Park, H. & Kaufman, L. J. In situ optical imaging of the growth of conjugated polymer aggregates. *Angew Chem. Int. Ed. Engl.* **57**, 1826–1830 (2018).
37. Park, H., Hoang, D. T., Paeng, K., Yang, J. & Kaufman, L. J. Conformation-dependent photostability among and within single conjugated polymers. *Nano Lett.* **15**, 7604–7609 (2015).
38. Lee, C. et al. Giant nonlinear optical responses from photon-avalanching nanoparticles. *Nature* **589**, 230–235 (2021).
39. Icha, J., Böning, D. & Türschmann, P. Precise and dynamic temperature control in high-resolution microscopy with VAHEAT. *Microscopy Today*. **30**, 34–41 (2022).
40. Kim, J. H., Schembri, T., Bialas, D., Stolte, M. & Würthner, F. Slip-stacked j-aggregate materials for organic solar cells and photodetectors. *Adv. Mater.* **34**, e2104678 (2021).
41. Hong, Y. et al. Efficient multiexciton state generation in charge-transfer-coupled perylene bisimide dimers via structural control. *J. J. Am. Chem. Soc.* **142**, 7845–7857 (2020).
42. Kennehan, E. R. et al. Using molecular vibrations to probe exciton delocalization in films of perylene diimides with ultrafast mid-IR spectroscopy. *Phys. Chem. Chem. Phys.* **19**, 24829–24839 (2017).
43. Tang, N. et al. Anomalous deep-red luminescence of perylene black analogues with strong π-π interactions. *Nat. Comm.* **14**, (2023).
44. Wang, Y., Ren, J. & Shuai, Z. Minimizing non-radiative decay in molecular aggregates through control of excitonic coupling. *Nat. Comm.* **14**, 5056 (2023).
45. Briseno, A. L. et al. Perylenediimide nanowires and their use in fabricating field-effect transistors and complementary inverters. *Nano Lett.* **7**, 2847–2853 (2007).

Acknowledgements

LJK and HK acknowledge support by the National Science Foundation under grant no. CHE-1807931. PJS and CL acknowledge support by the National Science Foundation under grant no. CHE-2203510. We thank Rachel Mow, Fay Ng, and Colin Nuckolls for assistance in ddPDI synthesis.

Author contributions

H.K. designed the research, collected data, performed analysis, and drafted the manuscript. C.L. collected data. P.J.S. obtained funding and provided supervision. L.J.K. obtained funding, provided supervision, performed analysis, and revised the manuscript. All authors reviewed the manuscript.

Declarations

Competing interests

The authors declare no competing interests.

Additional information

Supplementary Information The online version contains supplementary material available at https://doi.org/10.1038/s41598-024-83525-x.

Correspondence and requests for materials should be addressed to L.J.K.

Reprints and permissions information is available at www.nature.com/reprints.

Publisher's note Springer Nature remains neutral with regard to jurisdictional claims in published maps and institutional affiliations.